Boosting Sensing Performance of Vacancy-Containing Vertically Aligned MoS_2 Using rGO Particles

Rahul Kumar, Neeraj Goel, Abhay Vivek Agrawal, Ramesh Raliya, Saravanan Rajamani, Govind Gupta, Pratim Biswas, Mukesh Kumar, and Mahesh Kumar

***Abstract*— A design of an advanced sensing material, such as MoS_2, is imperative to enhance the sensing performance of a sensor. Because their usage alone for developing a practical sensor is impeditive owing to low gas response and slow response/recovery kinetics. Here, we report a high-performance NO_2 gas sensor using a hybrid of temperature-assisted sulfur vacancy within the edge-oriented vertically aligned MoS_2 (Sv-MoS_2) and crumpled reduced graphene oxide (rGO) particles. Interestingly, the Sv-MoS_2 functionalized by optimized rGO concentration exhibited a significant enhancement of response to NO_2 (approximately three times higher than that of pristine vertically aligned MoS_2) with fast response (<1 min) and complete recovery. Such a large improvement in the sensing performance could be attributed to controlled electrical/chemical sensitization level of MoS_2 through controllable vacancy and interface engineering. The vacancy engineering offers abundant active sites through creating sulfur vacancy in additionally rich edge active sites of vertically oriented MoS_2 for more electronic interaction with gas molecules. While interfacing of p-type rGO particles with n-type MoS_2 leads to multiple out-of-plane vertical nano-heterojunctions as a sensitizing configuration for boosting the performance of the sensor. This paper opens up a new approach towards improving the sensing activity of a 2D material via a synergistic vacancy and interface engineering.**

***Index Terms*— Vertical MoS_2, vacancy, rGO, charge transfer, NO_2 sensor.**

I. Introduction

OVER the last decade, the two dimensional (2D) materials offer the very promising platform to revolutionize the gas-sensing industry due to their large surface-to-volume ratio and ease of integration [1], [2]. Graphene has unveiled its great potential for electrochemical and gas-sensing applications, thereby enabling its uses in improving the efficiency and accuracy of smart sensing technologies. Due to its exceptionally low noise, sensors made up of graphene can detect even an individual gas molecule [3].

Analogous to graphene, transition metal dichalcogenides (TMDs) family member MoS_2 has been extensively studied as a potential gas sensing material because of its rich active sites (sulfur vacancy, defects, and edge sites). So far, the sensing ability of MoS_2 based sensors for detecting different gases and volatile organic compounds such as NO_2, NH_3, H_2, acetone, and ethanol have been thoroughly investigated [4]–[8] Although 2D layered MoS_2 has its inherent high surface-to-volume ratio for more electronic interaction in between target analyte and MoS_2, sensing performance also closely depends on its morphology, number of layers, exposed edge sites (edge sites are more chemically reactive compared to basal plane) and defects. Cho et al. have demonstrated that vertical aligned MoS_2 exhibits about 5 times higher sensitivity to NO_2 compared to that of horizontally aligned MoS_2.[9] The exposed edge sites of vertically aligned MoS_2 have high adsorption energy compared to that of terrace sites of horizontally aligned MoS_2.

Recently, interfacing of MoS_2 with metal nanoparticles, metal oxide semiconductor and other 2D materials open up new avenues towards improving the sensing performance due to chemical and electronic sensitization. For example, Kuru et al. reported that MoS_2 nanosheet–Pd nanoparticles composite based sensor shows high sensitivity to H_2 due to work function modulation of Pd nanoparticles [10]. Long et al. investigated that MoS_2/graphene hybrid aerogel exhibits better sensitivity to NO_2 with fast response/recovery times ($<$ 1 min) at 200°C compared to that of bare graphene [11]. Although, chemical functionalization and defect engineering have evolved as powerful techniques to tailor the electronic properties and enhance active sites of MoS_2 for a particular desired application. Nevertheless, most previously reported MoS_2 based gas sensor has been limited to explore a comprehensive joint effect of defect and interface engineering in sensing application.

In this work, we synthesized vertically aligned MoS_2 by using conventional chemical vapor deposition (CVD) method and created defect (sulfur vacancy) via a simple annealing

Manuscript received June 6, 2019; revised July 25, 2019; accepted July 25, 2019. Date of publication August 2, 2019; date of current version October 17, 2019. This work was supported by the Department of Science and Engineering Research Board (SERB) under Project SERB/F/2236/2015-16. The associate editor coordinating the review of this article and approving it for publication was Dr. Camilla Baratto. *(Corresponding author: Mahesh Kumar.)*

R. Kumar, N. Goel, S. Rajamani, and M. Kumar are with the Electrical Engineering Department, Indian Institute of Technology Jodhpur, Jodhpur 342037, India (e-mail: mkumar@iitj.ac.in).

A.V. Agrawal and M. Kumar are with the Department of Physics, Indian Institute of Technology Ropar, Rupnagar 140001, India.

R. Raliya and P. Biswas are with the Department of Energy, Environmental, and Chemical Engineering, Washington University in St. Louis, St. Louis, Missouri 63130 USA.

G. Gupta is with the Advanced Materials and Devices Division, CSIR-National Physical Laboratory (NPL), New Delhi 110012, India.

Digital Object Identifier 10.1109/JSEN.2019.2932106

process. Different crumpled rGO particles concentrations were loaded on the surface of MoS_2 and sulfur vacancy containing vertically aligned MoS_2(Sv-MoS_2) based device. Afterward, we investigated the sensing performance of the MoS_2, rGO/MoS_2, Sv-MoS_2 and rGO/Sv-MoS_2 devices to different NO_2 concentrations.

II. Experimental Section

The vertically aligned MoS_2 was synthesized on SiO_2/Si substrate by modified conventional chemical vapor deposition (CVD) process and details have been provided elsewhere [12]. Two different zirconia boats containing the two precursor sulfur (0.45 g) and MoO_3 (0.058 g) separately, were placed at the inlet and the closed end of the small tube, respectively. The small tube containing the boats was placed inside the bigger quartz tube in such a way that the MoO_3 was in zone 1 while the sulfur was in zone 2. The MoO_3 and S were annealed at two different temperatures of 800 and 350°C, respectively, at atmospheric pressure with Ar flow of 175 SCCM for 30 min and the substrate was put on the MoO_3 boat in face down position. Finally, the furnace was shut down and the tube was naturally cooled back to room temperature.

The modified Hummers method was used to synthesis of reduced graphene oxide (rGO) from first synthesized graphene oxide nanosheet [13]. In brief, a precursor powder of graphitic oxide was used to prepare graphene oxide nanosheet. The suspension was prepared in the water after treating the powder with sulfuric acid and potassium permanganate. Further, the residual permanganate was reduced after adding hydrogen peroxide in the suspension solution. To exfoliate the graphene oxide sheets, we filtered the suspension using 0.45-micron size filter and ultra-sonicated it. The repetitive filtration and centrifugation processes were used to obtain resultant sheets of graphene oxide. Finally, to obtain rGO having a desired concentration of oxygen functional group, these graphene oxide sheets were thermally reduced using Furnace Aerosol Reactor [14].

Characterization. The scanning electron microscopy (SEM, NOVA NANOSEM 450) and transmission electron microscopy (TEM, JEOL JEM-2100F) with accelerating voltage of 200 kV were performed to examine of morphology and crystal structure of primitive and hybrid of MoS_2 on SiO_2/Si substrate. The Raman spectroscopy (Renishaw single monochromator with laser excitation wavelength 514 nm) and X-ray photoelectron spectroscopy Scienta Omicron, Germany using monochromatized Al Kα (1486.7 eV) radiation source were used to analysis the charge transfers and sulfur vacancy in the hybrid of rGO and Sv-MoS_2.

The devices were fabricated by depositing two rectangular metal electrodes of Au/Cr (220/5 nm) on as-synthesized films by using thermal evaporation technique. The distance between two electrodes is 100 μm and width of electrode is 500 μm. The concentrations of rGO particles solution were 5, 10, and 15 mg/L (w/v) in the water at controlled physiological pH 7. A droplet of approximate 4 μL solution of each concentrated rGO solution was pipetted on the active surface area of the device and dried at 80 °C for 15 min before use it for further experiment. In this work, same active area of 5×10^{-4} cm^2 of the sensing material for rGO functionalization in all devices was used. The modulation in resistance of devices at constant 4 V under the exposure of gas was measured using Keithley 4200 semiconductor characterization system. In order to study the gas sensing behavior of the devices, gas sensing tests for all devices were performed in the same gas sensing chamber. The desired concentrations (ppm) of target gases were injected into the gas chamber.

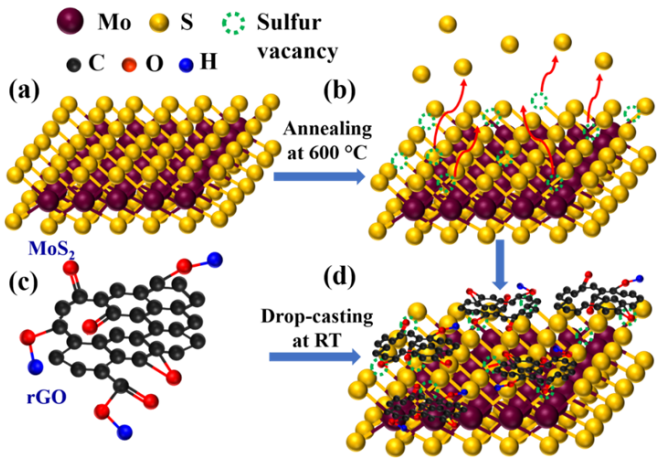

Fig. 1. Schematic representation of fabrication mechanism of rGO functionalized vacancy-engineered vertically aligned MoS_2 based device: (a) CVD grown vertically aligned MoS_2. (b) Annealing at 600°C induced sulfur vacancy in vertically aligned MoS_2. (c) rGO particles. (d) rGO functionalized on the surface of sulfur vacancy containing vertically aligned MoS_2.

III. Results and Discussion

Figs. 1 (a-d) illustrate the schematic for the fabrication of rGO/Sv-MoS_2 hybrids. First, edge-oriented vertically aligned MoS_2 was synthesized by using a modified tube in tube CVD process (see the experimental section). Afterward, the as-synthesized film was annealed at 600°C in high vacuum ambient for 40 min to induce sulfur vacancy. A number of sincere efforts have already been made to achieve the sulfur vacancy in MoS_2 in a controlled manner via thermal annealing [15]–[17].

Experimentally and theoretically, it has been proved that generation of sulfur vacancy is energetically favorable due to very low binding energy (2.12 eV) as compared to Mo vacancy (6.2 eV) [18]. This strategy strived to improve the chemical reactivity of vertically aligned MoS_2 through sulfur vacancy. Further, we decorated the different concentration of crumpled rGO particles on the surface of sulfur-vacancy containing vertical MoS_2 film (Sv-MoS_2). Finally, a resistive based sensor was fabricated by using the as-synthesized rGO/Sv-MoS_2 hybrids (an optical image given in Fig. S 1). Scanning electron microscopy (SEM) images in Figs. 2 (a) and (b) depict that the flakes are vertically aligned on the substrate and form a large uniformly interconnected 3-D network through interconnecting one another, indicating that a large number of edge sites of the MoS_2 are exposed. Figs. 2 (c) and (d) show the SEM images

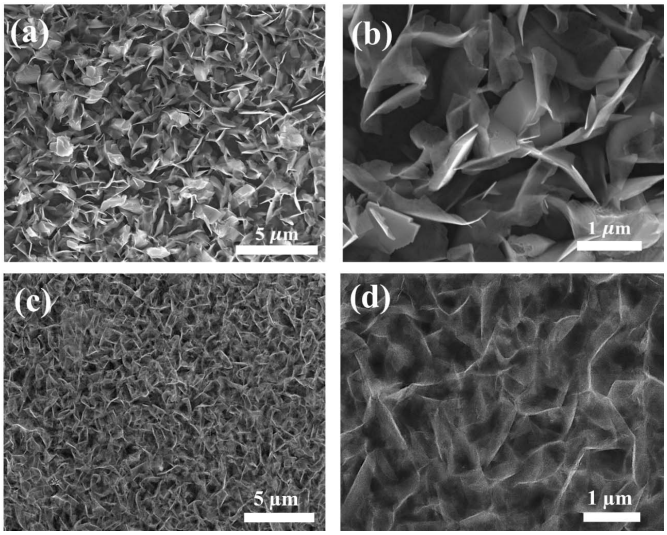

Fig. 2. SEM images of the pristine vertically aligned MoS_2 under (a) low, and (b) high magnifications. (c), and (d) SEM images of rGO functionalized vertically aligned Sv-MoS_2.

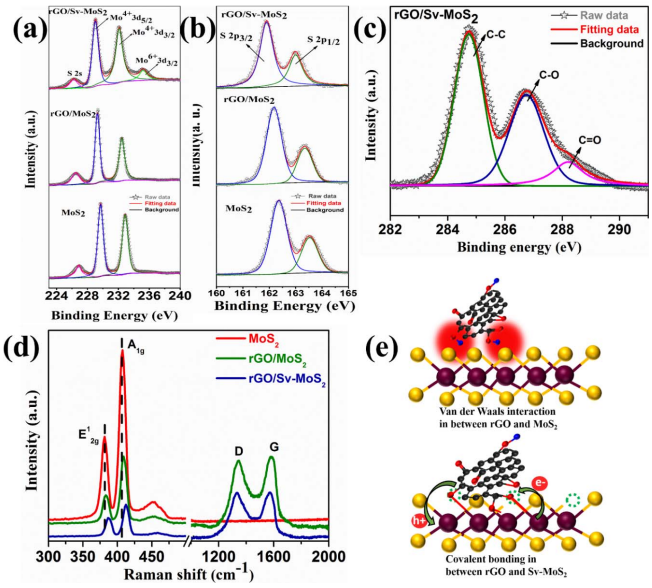

Fig. 3. High-resolution XPS spectras (a) for Mo 3d, (b) for S 2p, (c) for C 1s, and (d) Raman spectra of pristine MoS_2, rGO/MoS_2 and rGO/Sv-MoS_2. (e) The interaction of rGO particles with pristine and Sv-MoS_2.

of functionalized rGO particles on the surface of the Sv-MoS_2 and EDS mapping is shown in Fig. S 2.

In order to get a deeper insight into the crystal structure and decoration trend of the rGO particles on the MoS_2 network, transmission electron microscopy (TEM) experiment was performed (see supporting information). Further, X-ray photoelectron spectroscopy (XPS) and Raman spectroscopy were utilized to quantify the sulfur vacancy in the Sv-MoS_2 film and understanding of charge transfer mechanism at the rGO/Sv-MoS_2 interface. Figs. 3 (a) and (b) show the Mo 3d and S 2p peaks of pristine MoS_2, rGO/MoS_2 and rGO/Sv-MoS_2 hybrid. After the rGO decoration on pristine MoS_2 and Sv-MoS_2, the maxima of Mo 3d and S 2p peaks was shifted toward lower values of binding energy. The binding energy shifted to 229.1 from 229.6 and 232.4 eV from 232.8, corresponding to Mo $3d_{5/2}$ and Mo $3d_{3/2}$ orbitals of Mo^{4+} respectively, and to 161.9 from 162.3 and 163.1 from 163.4eV associated to S $2p_{3/2}$ and S $2p_{1/2}$ orbitals of divalent sulfide ions (S^{2-}) respectively, for the rGO/Sv-MoS_2 hybrid. The downshift in the position of the XPS peaks is directly ascribed to efficient electrons transfer from the Sv-MoS_2 to rGO, result in p-type doping in Sv-MoS_2 (Fermi level shift toward valance band), similar behavior has been observed in previous reports [19], [20]. Particularly, it was worth noting that one extra peak occurred at 235.2 eV in the deconvoluted Mo peaks, suggesting a strong chemical bonding in between rGO and Sv-MoS_2 by forming a bond between Mo and oxygen of rGO through sulfur vacancy position (Mo-O-C bonding). Because the exposed d-states of the under coordinated Mo atoms on sulfur vacancy sites facilitate chemical bonding with adsorbed species. The formation of Mo-O-C bonding at the interface of MoS_2 and graphene has been also seen in previous works [11], [21]. Further, to quantify the sulfur vacancy by using XPS data, S/Mo ratio was calculated as 1.97 and 1.73 for as-synthesized pristine MoS_2 and Sv-MoS_2, respectively, which confirmed a 13.5% concentration of sulfur vacancy in MoS_2 through thermal annealing, and this concentration is close to the optimal amount of sulfur vacancy in previous reported literature [22], [23]. Fig. 3 (c) illustrates the deconvolution of the high resolution peaks of C 1s in XPS spectra of the rGO/Sv-MoS_2 hybrid, which showed C 1s peaks at 284.7, 286.8, and 288.2 eV associated to C-C, C-O and C=O, respectively, indicating the presence of the oxygen functional groups in rGO.

Further, with the functionalization of rGO particles on pristine MoS_2 and Sv-MoS_2, a clear blue Raman shifts of the E^1_{2g} (382 cm^{-1}) and A_{1g} (407 cm^{-1}) peaks were observed (Fig. 3(d)). It is worth noting that blue Raman shift (4 cm^{-1}) was more in the rGO/Sv-MoS_2, suggesting p-type doping through efficient charge transfer via chemical bonding compared to that of van der Waals interaction in between rGO and pristine MoS_2 (Fig. 3(e)) [24]. Moreover, the two peaks at 1347 and 1587 cm^{-1} corresponding to D band and G band of rGO in the rGO/MoS_2, were shifted to 1340 and 1582 cm^{-1} respectively in the rGO/Sv-MoS_2. This red shifts suggested the n-type doping in the rGO through charge transfer at rGO/Sv-MoS_2 interface [25].

Fig. 4 (a) shows a linear behavior of I-V as an ohmic contact in between sensing layer (rGO decorated Sv-MoS_2) and the electrode at a temperature of 50 °C. It suggests that the sensor showed a gas response only due to intrinsic gas sensing characteristic of the rGO/Sv-MoS_2 hybrid and not because of electrode contacts. A temperature of 50 °C was selected after testing the operation temperature of the sensors from 25 to 150 °C. From Fig. S4 and table ST1, it is clear that high sensing performance such as higher response, acceptable response time and complete recovery at 50 °C temperature made it low optimal operating temperature value of the sensor.

Next, we investigated the dynamic-sensing response of pristine MoS_2, rGO/MoS_2, Sv-MoS_2 and rGO/Sv-MoS_2 devices to NO_2 exposure at low optimal operating temperature (50 °C)

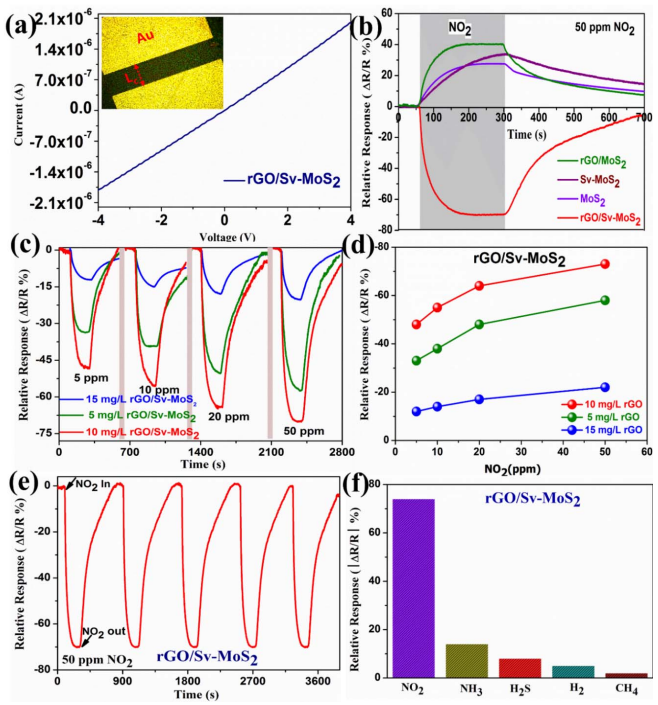

Fig. 4. (a) I-V measurement of the rGO/Sv-MoS_2 devices at a temperature of 50 °C, inset shows the optical image of the device. (b) Relative response versus time curves at low optimum operating temperature (50 °C) to 50 ppm NO_2 for the pristine MoS_2, Sv-MoS_2, rGO/MoS_2 and rGO/Sv-MoS_2 devices. (c) Transient response to NO_2 and, (d) relative response versus NO_2 concentration curves of the rGO/Sv-MoS_2 device for different concentrations of crumpled rGO at optimum operating temperature. (e) Cyclic test and, (f) Selectivity bar diagram of the rGO/Sv-MoS_2 device.

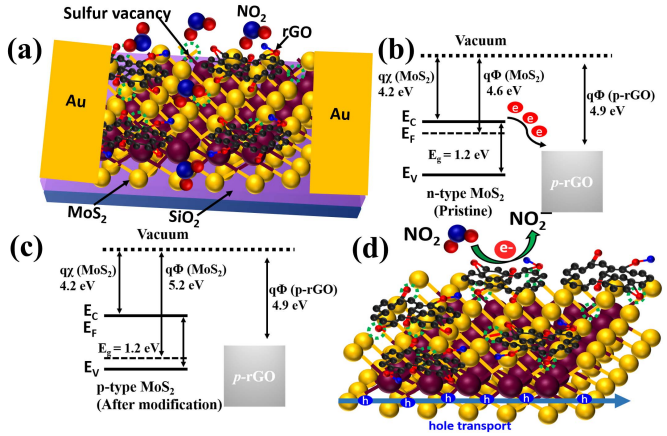

Fig. 5. (a) Schematic representation of a fabricated sensor by using crumpled rGO particles functionalized vacancy-engineered vertically aligned MoS_2. Energy band diagram of (b) n type-MoS_2 and rGO, (c) p-type MoS_2 and rGO (d) Sensing mechanism of the sensor.

(Fig. 4(b)). In this work, the relative response (sensitivity) of the devices was defined as $((R_g\text{-}R_o)/R_o)\times 100\%$, where R_g and R_o are the resistance of the devices in presence and absence of NO_2, respectively. Baseline resistance values for all sensors are shown in table ST2. As MoS_2 is n-type semiconductor and electrons were extracted by NO_2 from the surface of MoS_2 due to its oxidizing nature, thereby electrical resistance was increased in pristine MoS_2, rGO/MoS_2 and Sv-MoS_2 device. So, the MoS_2, Sv-MoS_2, and rGO/MoS_2 devices exhibited a positive relative response of $\sim$ 27, 34, and 39% to 50 ppm NO_2, respectively. In contrast, the electrical resistance of the rGO/Sv-MoS_2 device was effectively decreased upon exposure to NO_2 as shown in Fig. 4 (b). And, among all tested devices, the rGO/Sv-MoS_2 device exhibited drastically enhanced $\sim$ 72% relative response to 50 ppm NO_2. It is worth noting that the rGO particles were unable to make a p-type rGO/MoS_2 hybrid from the pristine n-type MoS_2, but they were sufficient to fabricate a p-type rGO/Sv-MoS2 hybrid due to more charge transfer in between rGO and temperature-assisted sulfur vacancy containing MoS_2. Point defects (sulfur vacancy) act as active centers to facilitate molecular adsorption and chemical functionalization. The oxygen atoms of rGO have strong binding energy of 2.395 eV on sulfur vacancy and show more effective charge transfer of 0.997 electron from sulfur vacancy to oxygen atom [26]. Therefore, efficient charge transfer was occurred in between rGO and Sv-MoS_2, which was sufficient to change n-type to p-type MoS_2 through hole injection by p-type rGO. Furthermore, in order to know the effect of rGO concentration on the surface of the Sv-MoS_2 for practical sensing applications, we measured the sensitivity of the device to various NO_2 concentrations from 5 to 50 ppm for different concentrations of the rGO particles (Fig. 4(c)). From Fig. 4(d), it was observed that relative response of the device was improved up to 10 mg/L solution of rGO and then dropped suddenly for 15 mg/L solution due to the formation of a continuous path of rGO film between two metal electrodes. Further, we calculated the theoretical detection limit on the basis of signal-to-noise ratio and NO_2 detection limits for pristine MoS_2 and the rGO/Sv-MoS_2 based sensor are about to be 18 and 172 ppb, respectively. Besides the high sensitivity of the device to NO_2, fast response/recovery kinetics with complete recovery at low operating temperature was also observed and the device exhibited a fast response of $\sim$56 s (Fig. S5) and complete recovery of $\sim$328 s as compared to pristine MoS_2 (response time $\sim$142 s and incomplete recovery). A high sensitivity, fast response and excellent reversibility make it inimitable from other NO_2 sensors based on different materials such as metal oxide semiconductors, and 2D materials (see table T1). The device also showed excellent repeatability without any significant expense of sensitivity for five consecutive cycles to 50 ppm NO_2, as shown in Fig. 4 (e). Finally, the selectivity of the sensor was examined toward different interfering gases such as NO_2, NH_3, H_2S, H_2, and CH_4. Fig. 4 (f) illustrates that the device showed a significantly higher sensitivity toward 50 ppm NO_2 compared to the sensitivity to 100 ppm concentration of each other aforementioned gases and transient gas responses of the sensor under exposing NH_3, H_2S, H_2, and CH_4 gas are shown in Fig. S6.

We discussed the gas sensing mechanism of our NO_2 gas sensor through the transient doping of the sensing material in the context of electronic interaction between target analytes and adsorption sites. In this sensor, the discrete p-type rGO particles act as a sensitizer for underlying carrier transporting channel of n-type MoS_2 and also as gas adsorption

TABLE I
COMPARISON BETWEEN PREVIOUSLY REPORTED NO_2 GAS SENSOR AND THIS WORK

Material	NO_2 Concentration	Temperature ($^\circ$C)	Sensitivity	Response Time	Recovery Time	Ref.
rGO/Sv-MoS_2	50 ppm	50	72 %[a]	56 s	328s	this work
MoS_2	50 ppm	50	27 % [a]	142 s	not recovered	this work
MoS_2	1000 ppm	RT	1372 % [a]	3 min	not recovered	[37]
Pt-MoS_2	1.2 ppm	RT	16 % [b]	30 min	>30 min	[7]
Graphene	2.5 ppm	RT	65 % [b]	1400 s	1500 s	[38]
MoS_2/Graphene	0.5 ppm	200	10 % [a]	< 1 min	< 1 min	[11]
MoS_2/SnO_2	10 ppm	RT	28 % [c]	6.8 min	2.7 min	[33]
MoS_2	10 ppm	UV@ RT	25.3 % [d]	-	44 s	[39]
MoS_2/PbS	100 ppm	RT	23 % [a]	30 s	235 sec	[40]
MoS_2 hollow sphere	100 ppm	150	40.3 % [a]	79 s	225 sec	[41]
MoS_2 on SiO_2 NRs	50 ppm	RT	390 % [a]	-	not recovered	[42]
ZnO Nanorods	100 ppm	200	662% [a]	35 s	206 s	[43]

[a] $(R_g - R_o)/R_o \times 100\%$, [b] $(I_g - I_o)/I_o \times 100\%$, [c] $(\Delta G/G_o) \times 100\%$, [d] R_g/R_o

centers (Fig. 5(a)). The electron affinity of the MoS_2 is 4.2 eV [27], [28] and Fermi energy of the rGO and MoS_2 are 4.9 and 4.6 eV, respectively [27], [29], [30], resulting in band bending at the interface between rGO and MoS_2 due to energy offset (Fig. 5(b)). Therefore, due to difference in Fermi levels electrons tend to move from the MoS_2 to rGO, leading to an increased hole concentration and inducing a p-type semiconducting behavior in the transporting channel of Sv-MoS_2 and energy band diagram of p-type modified MoS_2 and rGO is shown in Fig. 5(c). Thus, conduction of the sensor is mainly influenced by the degree of perturbation of the hole concentration in the p-type transporting channel (Sv-MoS_2).

Upon exposure to NO_2, electrons transfer from rGO to the NO_2. The depletion of electrons shifted the Fermi level of rGO towards the valance band [31], resulting in an increased energy offset, which causes more electron transfer from the MoS_2 to rGO or hole injection by rGO into Sv-MoS_2. Moreover, the hole concentration in transporting channel was further increased through electrons extraction by NO_2 adsorption on the rich active sites (sulfur vacancy, dangling bond at the edge) of the Sv-MoS_2. Since, the transporting channel of Sv-MoS_2 in the rGO/Sv-MoS_2 hybrids demonstrates p-type behavior as shown in Fig. 5(d), the Fermi level shifts towards valance band due to electron transfer, causing enhancement in the current of the sensor. Consequently, sensitivity of the rGO/Sv-MoS_2 device to NO_2 gas was enhanced. Previous studies have also been showed that a p-type MoS_2 as a transporting layer of the sensor exhibits good sensing performance to NO_2 [7], [32], [33]. On the other hand, oxygen-containing functional groups in the rGO play a key role to achieve complete recovery with fast response at low operating temperature.[34] At recovery step oxygen molecules oxidize to hydroquinone into quinones [35], thereby oxygen converts in O^-_{ads} ($O_{2\,gas} + e \rightarrow 2O^-_{ads}$), which assist to desorb the gas molecules at room temperature ($NO^-_{2\,ads} + O^-_{ads} \rightarrow NO_2$ gas $+ O^{2-}_{ads}$) [36]. Moreover, hydroxyl groups rotate and relaxed to their original states during the adsorption and desorption of NO_2 molecules, respectively, leading to reversible NO_2 sensing of the rGO/Sv-MoS_2 device[34]. As a result, the improved sensing performance of the rGO/Sv-MoS_2 hybrid is attributed to a synergistic effect of the abundance reactive sites of the Sv-MoS_2 and chemical/electronic sensitization by rGO particles.

IV. CONCLUSION

We have successfully fabricated and demonstrated a high-performance NO_2 sensor based on activated and optimized vertically aligned MoS_2 by vacancy and interface engineering. Our sensing results show that the rGO/Sv-MoS_2 device exhibited superior relative response with fast response/recovery kinetics as well as excellent selectivity toward NO_2 against many other toxic and combustible gases than other MoS_2, Sv-MoS_2 and rGO/MoS_2 devices.

REFERENCES

[1] S.-Y. Cho *et al.*, "Superior chemical sensing performance of black phosphorus: Comparison with MoS_2 and graphene," *Adv. Mater.*, vol. 28, no. 32, pp. 7020–7028, Aug. 2016.
[2] C. N. R. Rao, K. Gopalakrishnan, and U. Maitra, "Comparative study of potential applications of graphene, MoS_2, and other two-dimensional materials in energy devices, sensors, and related areas," *ACS Appl. Mater. Interfaces*, vol. 7, no. 15, pp. 7809–7832, Mar. 2015.
[3] F. Schedin *et al.*, "Detection of individual gas molecules adsorbed on graphene," *Nature Mater.*, vol. 6, no. 9, p. 652, Sep. 2007.
[4] K. Lee, R. Gatensby, N. McEvoy, T. Hallam, and G. S. Duesberg, "High-performance sensors based on molybdenum disulfide thin films," *Adv. Mater.*, vol. 25, no. 46, pp. 6699–6702, 2013.
[5] F. K. Perkins, A. L. Friedman, E. Cobas, P. M. Campbell, G. G. Jernigan, and B. T. Jonker, "Chemical vapor sensing with monolayer MoS_2," *Nano Lett.*, vol. 13, no. 2, pp. 668–673, Jan. 2013.
[6] R. Kumar, N. Goel, and M. Kumar, "UV-activated MoS_2 based fast and reversible NO_2 sensor at room temperature," *ACS Sensors*, vol. 2, no. 11, pp. 1744–1752, Nov. 2017.
[7] H. Qiyuan *et al.*, "Fabrication of flexible MoS_2 thin-film transistor arrays for practical gas-sensing applications," *Small*, vol. 8, no. 19, pp. 2994–2999, Oct. 2012.
[8] K. Rahul *et al.*, "Growth of MoS_2-MoO_3 hybrid microflowers via controlled vapor transport process for efficient gas sensing at room temperature," *Adv. Mater. Interfaces*, vol. 5, no. 10, May 2018, Art. no. 1800071.

[9] S.-Y. Cho *et al.*, "Highly enhanced gas adsorption properties in vertically aligned MoS_2 layers," *ACS Nano*, vol. 9, no. 9, pp. 9314–9321, Aug. 2015.

[10] C. Kuru *et al.*, "MoS_2 nanosheet-Pd nanoparticle composite for highly sensitive room temperature detection of hydrogen," *Adv. Sci.*, vol. 2, no. 4, Apr. 2015, Art. no. 1500004.

[11] L. Hu *et al.*, "High surface area MoS_2/graphene hybrid aerogel for ultrasensitive NO_2 detection," *Adv. Funct. Mater.*, vol. 26, no. 28, pp. 5158–5165, Jul. 2016.

[12] A. V. Agrawal *et al.*, "Controlled growth of MoS_2 flakes from in-plane to edge-enriched 3D network and their surface-energy studies," *ACS Appl. Nano Mater.*, vol. 1, no. 5, pp. 2356–2367, Apr. 2018.

[13] Y. Jiang, R. Raliya, J. D. Fortner, and P. Biswas, "Graphene oxides in water: Correlating morphology and surface chemistry with aggregation behavior," *Environ. Sci. Technol.*, vol. 50, no. 13, pp. 6964–6973, Jun. 2016.

[14] Y. Jiang, R. Raliya, P. Liao, P. Biswas, and J. D. Fortner, "Graphene oxides in water: Assessing stability as a function of material and natural organic matter properties," *Environ. Sci. Nano*, vol. 4, no. 7, pp. 1484–1493, 2017.

[15] L. Mengxi *et al.*, "Temperature-triggered sulfur vacancy evolution in monolayer MoS_2/graphene heterostructures," *Small*, vol. 13, no. 40, Oct. 2017, Art. no. 1602967.

[16] M. Donarelli, F. Bisti, F. Perrozzi, and L. Ottaviano, "Tunable sulfur desorption in exfoliated MoS_2 by means of thermal annealing in ultra-high vacuum," *Chem. Phys. Lett.*, vol. 588, pp. 198–202, Nov. 2013.

[17] S. Tongay *et al.*, "Defects activated photoluminescence in two-dimensional semiconductors: Interplay between bound, charged, and free excitons," *Sci. Rep.*, vol. 3, Sep. 2013, Art. no. 2657.

[18] J. Hong *et al.*, "Exploring atomic defects in molybdenum disulphide monolayers," *Nature Commun.*, vol. 6, Feb. 2015, Art. no. 6293.

[19] J. Suh *et al.*, "Doping against the native propensity of MoS_2: Degenerate hole doping by cation substitution," *Nano Lett.*, vol. 14, no. 12, pp. 6976–6982, Nov. 2014.

[20] T. Alexey *et al.*, "Controlled doping of large-area trilayer MoS_2 with molecular reductants and oxidants," *Adv. Mater.*, vol. 27, no. 7, pp. 1175–1181, Feb. 2015.

[21] Y. Teng *et al.*, "MoS_2 nanosheets vertically grown on graphene sheets for lithium-ion battery anodes," *ACS Nano*, vol. 10, no. 9, pp. 8526–8535, Aug. 2016.

[22] H. Li *et al.*, "Activating and optimizing MoS_2 basal planes for hydrogen evolution through the formation of strained sulphur vacancies," *Nature Mater.*, vol. 15, pp. 48–53, Nov. 2015.

[23] J. Li *et al.*, "Boosting hydrogen evolution performance of MoS_2 by band structure engineering," *Adv. Mater. Interfaces*, vol. 4, no. 16, Aug. 2017, Art. no. 1700303.

[24] B. Chakraborty, A. Bera, D. V. S. Muthu, S. Bhowmick, U. V. Waghmare, and A. K. Sood, "Symmetry-dependent phonon renormalization in monolayer MoS_2 transistor," *Phys. Rev. B, Condens. Matter*, vol. 85, no. 16, Apr. 2012, Art. no. 161403.

[25] S. Some *et al.*, "Highly air-stable phosphorus-doped n-type graphene field-effect transistors," *Adv. Mater.*, vol. 24, no. 40, pp. 5481–5486, Oct. 2012.

[26] H. Nan *et al.*, "Strong photoluminescence enhancement of MoS_2 through defect engineering and oxygen bonding," *ACS Nano*, vol. 8, no. 6, pp. 5738–5745, May 2014.

[27] M. S. Choi *et al.*, "Controlled charge trapping by molybdenum disulphide and graphene in ultrathin heterostructured memory devices," *Nature Commun.*, vol. 4, Mar. 2013, Art. no. 1624.

[28] C. Gong, H. Zhang, W. Wang, L. Colombo, R. M. Wallace, and K. Cho, "Band alignment of two-dimensional transition metal dichalcogenides: Application in tunnel field effect transistors," *Appl. Phys. Lett.*, vol. 103, no. 5, Jul. 2013, Art. no. 53513.

[29] B. Kang, S. Lim, W. H. Lee, S. B. Jo, and K. Cho, "Work-function-tuned reduced graphene oxide via direct surface functionalization as source/drain electrodes in bottom-contact organic transistors," *Adv. Mater.*, vol. 25, no. 41, pp. 5856–5862, Nov. 2013.

[30] M. S. Choi *et al.*, "Lateral MoS_2 p–n junction formed by chemical doping for use in high-performance optoelectronics," *ACS Nano*, vol. 8, no. 9, pp. 9332–9340, Aug. 2014.

[31] J. D. Fowler, M. J. Allen, V. C. Tung, Y. Yang, R. B. Kaner, and B. H. Weiller, "Practical chemical sensors from chemically derived graphene," *ACS Nano*, vol. 3, no. 2, pp. 301–306, Feb. 2009.

[32] M. A. Worsley *et al.*, "3D MoS_2 aerogel for ultrasensitive NO_2 detection and its tunable sensing behavior," *Adv. Mater. Interfaces*, vol. 4, no. 16, Aug. 2017, Art. no. 1700217.

[33] S. Cui, Z. Wen, X. Huang, J. Chang, and J. Chen, "Stabilizing MoS_2 nanosheets through SnO_2 nanocrystal decoration for high-performance gas sensing in air," *Small*, vol. 11, no. 19, pp. 2305–2313, May 2015.

[34] Y. R. Choi *et al.*, "Role of oxygen functional groups in graphene oxide for reversible room-temperature NO_2 sensing," *Carbon*, vol. 91, pp. 178–187, Sep. 2015.

[35] H. Vedala, D. C. Sorescu, G. P. Kotchey, and A. Star, "Chemical sensitivity of graphene edges decorated with metal nanoparticles," *Nano Lett.*, vol. 11, no. 6, pp. 2342–2347, May 2011.

[36] R. Kumar, O. Al-Dossary, G. Kumar, and A. Umar, "Zinc oxide nanostructures for NO_2 gas–sensor applications: A review," *Nano-Micro Lett.*, vol. 7, no. 2, pp. 97–120, Apr. 2015.

[37] D. J. Late *et al.*, "Sensing behavior of atomically thin-layered MoS_2 transistors," *ACS Nano*, vol. 7, no. 6, pp. 4879–4891, May 2013.

[38] S. Kumar, S. Kaushik, R. Pratap, and S. Raghavan, "Graphene on paper: A simple, low-cost chemical sensing platform," *ACS Appl. Mater. Interfaces*, vol. 7, no. 4, pp. 2189–2194, Jan. 2015.

[39] Y. Kang, S. Pyo, E. Jo, and J. Kim, "Light-assisted recovery of reacted MoS_2 for reversible NO_2 sensing at room temperature," *Nanotechnology*, vol. 30, no. 35, Jun. 2019, Art. no. 355504.

[40] X. Xin *et al.*, "Enhanced performances of PbS quantum-dots-modified MoS_2 composite for NO_2 detection at room temperature," *ACS Appl. Mater. Interfaces*, vol. 11, no. 9, pp. 9438–9447, Mar. 2019.

[41] Y. Li *et al.*, "Hierarchical hollow MoS_2 microspheres as materials for conductometric NO_2 gas sensors," *Sens. Actuators B, Chem.*, vol. 282, pp. 259–267, Mar. 2019.

[42] Y.-S. Shim *et al.*, "Synthesis of numerous edge sites in MoS_2 via SiO_2 nanorods platform for highly sensitive gas sensor," *ACS Appl. Mater. Inter.*, vol. 10, no. 37, pp. 31594–31602, Aug. 2018.

[43] Y. H. Navale *et al.*, "Zinc oxide hierarchical nanostructures as potential NO_2 sensors," *Sens. Actuators, B Chem.*, vol. 251, no. 2, pp. 551–563, Nov. 2017.

Rahul Kumar received the B.Tech. degree in electronics and communication engineering from Uttar Pradesh Technical University, Lucknow, India, and the M.Tech. degree in material science and technology from the Indian Institute of Technology (BHU) Varanasi, India. He is currently pursuing the Ph.D. degree in electrical engineering with IIT Jodhpur, India.

His research interests include synthesis of TMDCs using CVD and 2-D materials based gas sensors and photodetectors.

Neeraj Goel received the B.Tech. degree in electronics and communication engineering from Uttar Pradesh Technical University, Lucknow, India, and the M.Tech. degree in electronics and communication engineering from IIT (ISM) Dhanbad, Dhanbad, India. He is currently pursuing the Ph.D. degree in electrical engineering with IIT Jodhpur, Jodhpur, India.

His current research interests include 2-D materials-based photodetectors and gas sensors.

Abhay Vivek Agrawal received the bachelor's and master's degrees in physics from Aligarh Muslim University. He is currently pursuing the Ph.D. degree with the Physics Department, Indian Institute of Technology Ropar, India.

His current research interests are synthesis and study of electrical and optical properties of MoS_2 and its application in gas sensing.

Ramesh Raliya received the Ph.D. degree from the Central Arid Zone Research Institute, Jodhpur, India.

He is a Research Scientist with the Department of Energy, Environmental, and Chemical Engineering, Washington University in St. Louis, USA. His current research interests are synthesizing novel inorganic and organic nanomaterials with independently controlled properties and *in-vitro* and *in vivo* biosynthesis, sol-gel, aerosol, and physical synthesis approaches.

Saravanan Rajamani received the Ph.D. degree in electronic engineering from Roma Tre University, Rome.

He is currently an SERB-National Post-Doctoral Fellow with the Department of Electrical Engineering, Indian Institute of Technology Jodhpur. His current research interests are optoelectronic materials and devices.

Govind Gupta is currently a Principal Scientist and an Associate Professor (AcSIR) with the Advanced Materials and Device Metrology Division, CSIR-National Physical Laboratory, New Delhi, India. His research interests include development of solid state gas sensors, III-Nitride systems, surface & interface physics.

Pratim Biswas received the Ph.D. degree from the California Institute of Technology, USA.

He is a Professor with the Department of Energy, Environmental, and Chemical Engineering, Washington University in St. Louis, USA. His research interests include aerosol science and engineering, nanoparticle technology, environmental nanotechnology, and the thermal sciences.

Mukesh Kumar received the Ph.D. degree in physics from IIT Delhi, India.

He was with South Dakota State University, the Colorado School of Mines, and the National Center for Photovoltaics, USA, from 2010 to 2013. He is currently an Assistant Professor with the Department of Physics, Indian Institute of Technology Ropar, India. His current researches focus on kesterites and chalcopyrites materials, polymer BHJ, perovskite solar cells, transparent conducting electrodes, and sensors development.

Mahesh Kumar received the M.Tech. degree in solid state materials from IIT Delhi and the Ph.D. degree from IISc Bangalore.

He is an Assistant Professor with the Department of Electrical Engineering, Indian Institute of Technology Jodhpur, Jodhpur, India. His area of research interests are electronic materials, semiconductor devices, thin films and nanostructures of wide band gap semiconductors.